PNAS
www.pnas.org

Supplementary Information for

Arrhythmia mutations in Calmodulin cause conformational changes that affect interactions with the cardiac voltage-gated calcium channel

Kaiqian Wang, Christian Holt, Jocelyn Lu, Malene Brohus, Kamilla Taunsig Larsen, Michael Toft Overgaard, Reinhard Wimmer, Filip Van Petegem

Reinhard Wimmer
Email: rw@bio.aau.dk

Filip Van Petegem
Email: filip.vanpetegem@gmail.com

This PDF file includes:

Other supplementary materials for this manuscript include the following:

SUPPLEMENTARY METHODS

TAMRA fluorescence anisotropy experiments.

For each row-wise titration curve (i.e. each $[Ca^{2+}]_{free}$) a CaM-$Ca_V1.2$ IQ K_D was obtained by non-linear curve fitting in GraphPad Prism 6 to the quadratic one-site binding equation:

$$Y = \frac{[PCaM]}{[P]_{tot}} = \frac{K_D + [P]_{tot} + [CaM]_{tot}}{2 \cdot [P]_{tot}} - \sqrt{\left(\frac{K_D + [P]_{tot} + [CaM]_{tot}}{2 \cdot [P]_{tot}}\right)^2 - \frac{[CaM]_{tot}}{[P]_{tot}}}$$

Where Y is the fractional saturation of peptide, and $[P]_{tot}$ and $[CaM]_{tot}$ are the total concentrations of peptide and CaM, respectively.

For the highest CaM concentration (column 1 in the plate) we extracted Ca^{2+} binding curves for each of the CaM:IQ complexes. A Ca^{2+} K_D for each complex was obtained by non-linear fitting in GraphPad Prism 6 to the Hill equation:

$$\theta = \frac{1}{\left(\frac{K_D}{[Ca^{2+}]_{free}}\right)^n + 1}$$

Where θ is the fractional saturation of the CaM:IQ complex with Ca^{2+}, n the Hill coefficient, and K_D is the $[Ca^{2+}]_{free}$ where θ = 0.5.

The free Ca^{2+} concentration was verified in full plates of titrations at least once for each batch of low and high Ca^{2+} stock solutions, by use of the Ca^{2+}-sensitive probe Fura-2 (Invitrogen Molecular Probes). The average difference between calculated and determined free Ca^{2+} concentrations were lower than 10% in the appropriate range for Fura-2 (sub nM to ~5uM). Consistency over time was further ensured by regular re-evaluation of the Ca^{2+} dependent WT CaM:TAMRA-peptide dissociation constants.

Crystallization conditions.

Crystals were obtained by hanging-drop vapor diffusion by mixing equal volumes of protein (~30mg/ml) and reservoir solution. Crystals of N97S Ca^{2+}/CaM appeared in a solution of 20 % PEG 3350 (w/v) and 0.1 M BIS-TRIS, pH 6.5, at 4 ºC. Complexes of D95V Ca^{2+}/CaM:IQ domain were crystallized in a solution of 1 M LiCl, 30 % PEG 6000 (w/v), and 0.1 M Bicine, pH 10.3, at 4 ºC. Crystals of the N97I Ca^{2+}/CaM:IQ domain complex appeared in a solution of 2.1 M sodium malonate and 0.1 M HEPES, pH 7.5, at 25 ºC. The F141L Ca^{2+}/CaM:IQ domain complex crystallized in a solution of 0.5 M potassium nitrate and 20 % PEG 3350 (w/v) at 25 ºC.

NMR experiments.

Wild-type apoCaM: 1.2 mM CaM, 10 mM EDTA, 10 mM KCl, 2 mM HEPES (4-(2-hydroxyethyl)-1-piperazineethanesulfonic acid), 2 mM NaN_3, pH 6.53, 0.1 mM TSP-d_4

(sodium 2,2,3,3-tetradeutero, 3-(trimethylsilyl) propionate) dissolved in 95 % H_2O, 5 % D_2O.
Wild-type Ca_4-CaM: 0.15 mM CaM, 5 mM $CaCl_2$, 10 mM KCl, 2 mM HEPES, 2 mM NaN_3, pH 6.52, 0.1 mM TSP-d_4 dissolved in 95 % H_2O, 5 % D_2O.
D95V Ca_4-CaM: 1.2 mM D95V CaM, 5 mM $CaCl_2$, 10 mM KCl, 2 mM, 2 mM NaN_3, pH 6.55, 0.1 mM TSP-d_4 dissolved in 95 % H_2O, 5 % D_2O.
F141L apoCaM: 0.58 mM F141L CaM, 10 mM EDTA, 10 mM KCl, 2 mM HEPES, 2 mM NaN_3, pH 6.55, 0.1 mM TSP-d_4 dissolved in 95 % H_2O, 5 % D_2O.
F141L Ca_4-CaM: 0.53 mM F141L CaM, 10 mM $CaCl_2$, 10 mM KCl, 2 mM HEPES, 2 mM NaN_3, pH 6.45, 0.1 mM TSP-d_4 dissolved in 95 % H_2O, 5 % D_2O.

All NMR spectra, if not specified otherwise, were recorded on a BRUKER AVIII-600 MHz spectrometer equipped with a CPP-TCI probe. Spectra were acquired at 298.1 K. BRUKER TopSpin 3.5pl6 was used for recording and processing. The following spectra were acquired: 2D-^{15}N-HSQC, 2D-^{13}C HSQC (constant-time for aliphatic and constant-time TROSY for aromatic carbon atoms), 3D-^{15}N-edited TOCSY (50 ms mixing), C-detected CACO and NCO, CBCA(CO)NH, HBHA(CBCACO)NH, (H)C(CCCO)NH, H(CCCO)NH, HNCA, BEST-HNCACB, HNCO, HN(CA)CO, (HB)CB(CGCD)HD, (HB)CB(CGCDCE)HE, 3D-^{15}N-edited NOESY (70 ms mixing), 3D-^{13}C-edited NOESY for aliphatic carbon atoms (75 ms mixing) and 3D-^{13}C-edited NOESY for aromatic carbon atoms (100 ms mixing time) and an experiment for determining ^{15}N-T_1, ^{15}N-T_2 and the [^{1}H]-^{15}N NOE(1). T_2 relaxation dispersion was measured for F141L apoCaM using the BRUKER standard pulse program hsqcrexetf3gpsi3d(2) with a constant relaxation delay τ_{CPMG} of 50 ms (2 x 25 ms) and CPMG field strengths ranging from 0 to 1200 Hz (20, 40, 60,80, 100, 120, 140, 160, 200, 260, 320, 500, 600, 700, 800, 900, 1000 and 1200 Hz with repetitions at 40, 80, 120, 160, 260, 500, 700, 900 and 1200 Hz), acquired in random order in an interleaved manner recording a full cycle of field strengths for each individual scan at a time.

[^{1}H,^{15}N]-HSQC spectra of F141L apoCaM were acquired at 277.1, 298.1 and 310.1 K at both above mentioned 600 MHz and a BRUKER AVIII-950 MHz spectrometer with a 5mm TCI probe.

Relaxation data were analyzed with BRUKER's Protein Dynamics Center v. 2.3 and 2.5.4, except for T_2 relaxation dispersion data, which were fitted with Mathematica v 11.1.

The 3D-structures of the F141L apo and Ca^{2+}/CaM were determined using standard methodology.

F141L apoCaM: CcpNmr Analysis 2.4.2(3) was used to obtain the backbone and side-chain resonance assignment of most atoms. The NOESY cross peaks were integrated and exported from CcpNmr. The TALOS-N web server(4) was used to derive backbone dihedral angle constraints from the chemical shifts obtained. Dihedral angle constraints and integrated NOESY peak lists were provided to CYANA 3.97(5-8) for automated NOESY assignment and to calculate 100 structures.

F141L Ca_4-CaM: CARA 1.8.4 (ref(9)) was used to obtain the backbone and side-chain resonance assignment of most atoms. The NEASY module was used to collect and integrate NOESY cross peaks. The TALOS-N web server(4) was used to derive backbone dihedral angle constraints from the chemical shifts obtained. Dihedral angle constraints and integrated and assigned NOESY peak lists were provided to CYANA 3.97 to calculate 100 structures. Calcium ions were included into the calculation by assuming identical Calcium-binding modes as for the wild-type. The calcium coordination from PDB ID 1CLL was translated to restraints, that were provided as input for the structure calculation, by measuring the actual distance between the Calcium atom and its coordination partner and providing this distance ± 0.2 Å as distance restraint. The restraints have been deposited at the PDB database along with the structure.
Structure refinement (both F141L apoCaM and F141L Ca^{2+}/CaM): The 20 structures with lowest residual target function were retained for refinement with YASARA 18.2.7 (ref(10)). Refinement was done in two steps: first, *in vacuo* using the NOVA force field(11), subsequently in water using the YASARA force field(12). The resulting 20 structures were sorted by ascending residual violation energies and submitted to the PDB database. Parameters for the structure determination are shown in Table S4.

SUPPLEMENTARY FIGURES

Figure S1

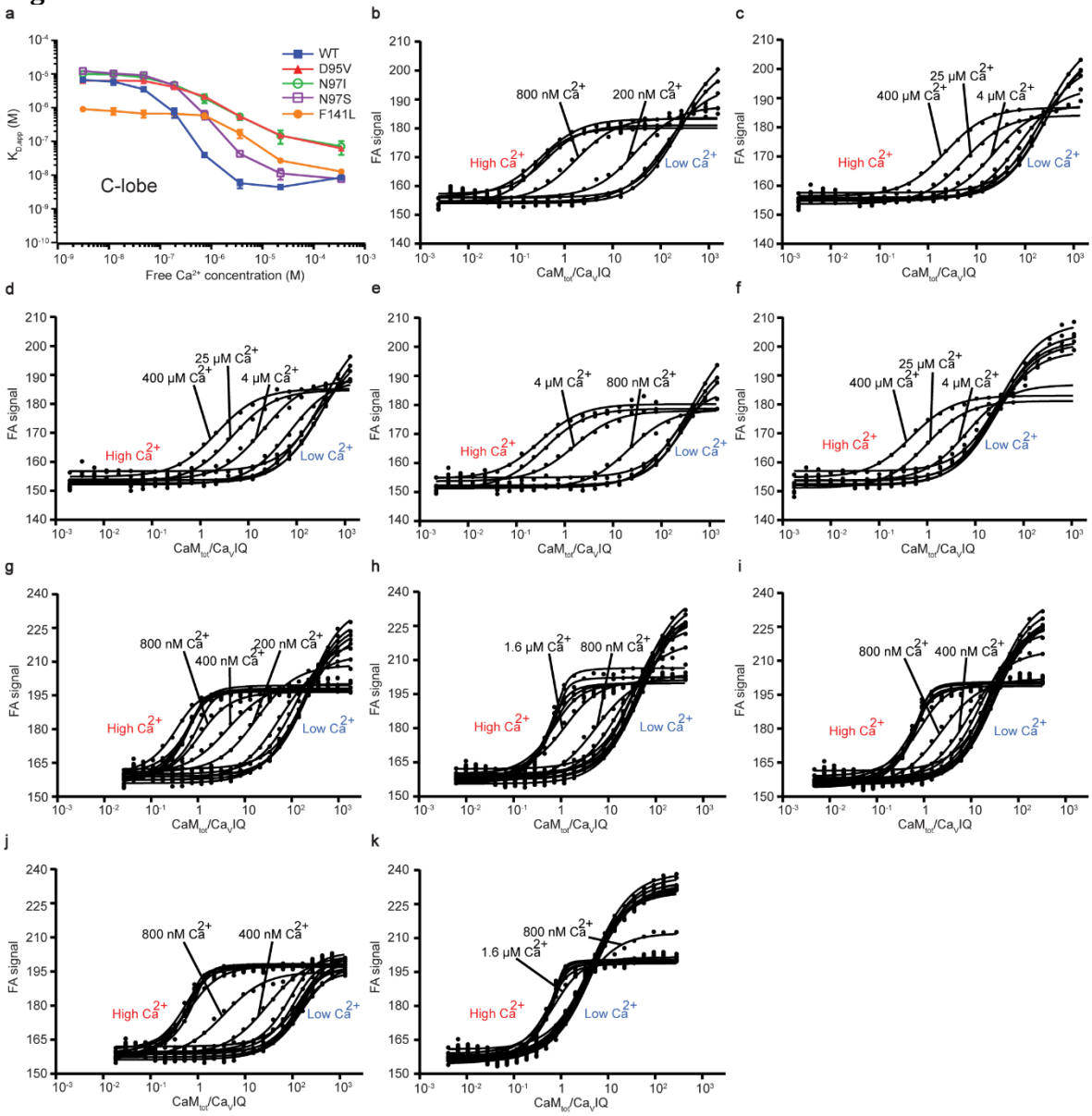

Supplementary Figure 1 Characterization of CaM and C-lobe:$Ca_V1.2$ IQ domain interactions by fluorescence anisotropy. **(a)** Binding affinity ($K_{D,app}$) of C-lobe variants to the IQ domain at various free calcium concentrations. Error bars represent the standard deviation of three replicates. TAMRA fluorescence anisotropy (FA) signal observed upon titration of **(b)** WT C-lobe, **(c)** D95V C-lobe, **(d)** N97I C-lobe, **(e)** N97S C-lobe, **(f)** F141L C-lobe, **(g)** Wild-type CaM, **(h)** D95V CaM, **(i)** N97I CaM, **(j)** N97S CaM, and **(k)** F141L CaM into TAMRA-labelled IQ domain over 16 free Ca^{2+} concentrations. Curves were fit to a quadratic one-site binding equation. Experiments were conducted in triplicates; representative curves are shown.

Figure S2

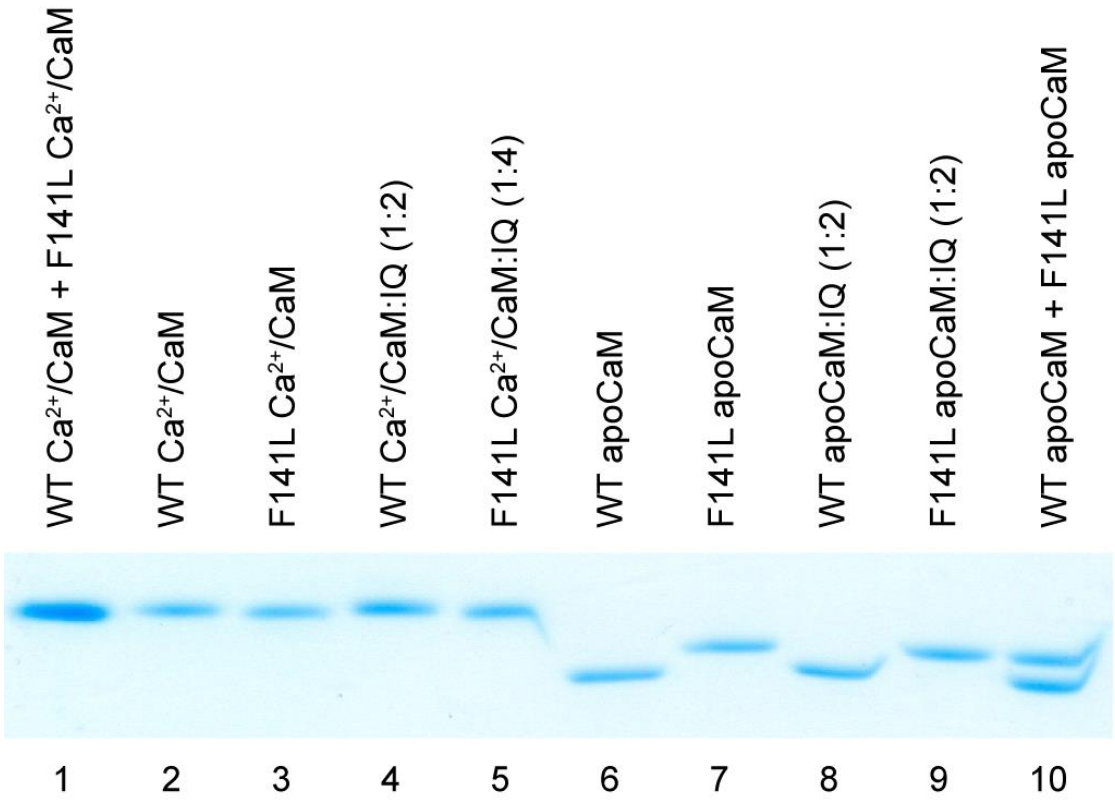

Supplementary Figure 2. Native PAGE of wild-type and F141L CaM. Shown are various lanes in the presence and absence of Ca^{2+} and in the presence and absence of IQ domain. Under Ca^{2+} conditions, no difference is visible between wild-type and F141L, but a significant shift in mobility is visible for F141L, relative to wild-type CaM, under Ca^{2+}-free conditions. This shift persists in the presence of IQ domain. This is highlighted in lane 10, which contains a mixture of wild-type and F141L CaM. These results suggest a major conformational change, induced by F141L, under Ca^{2+}-free conditions.

Figure S3

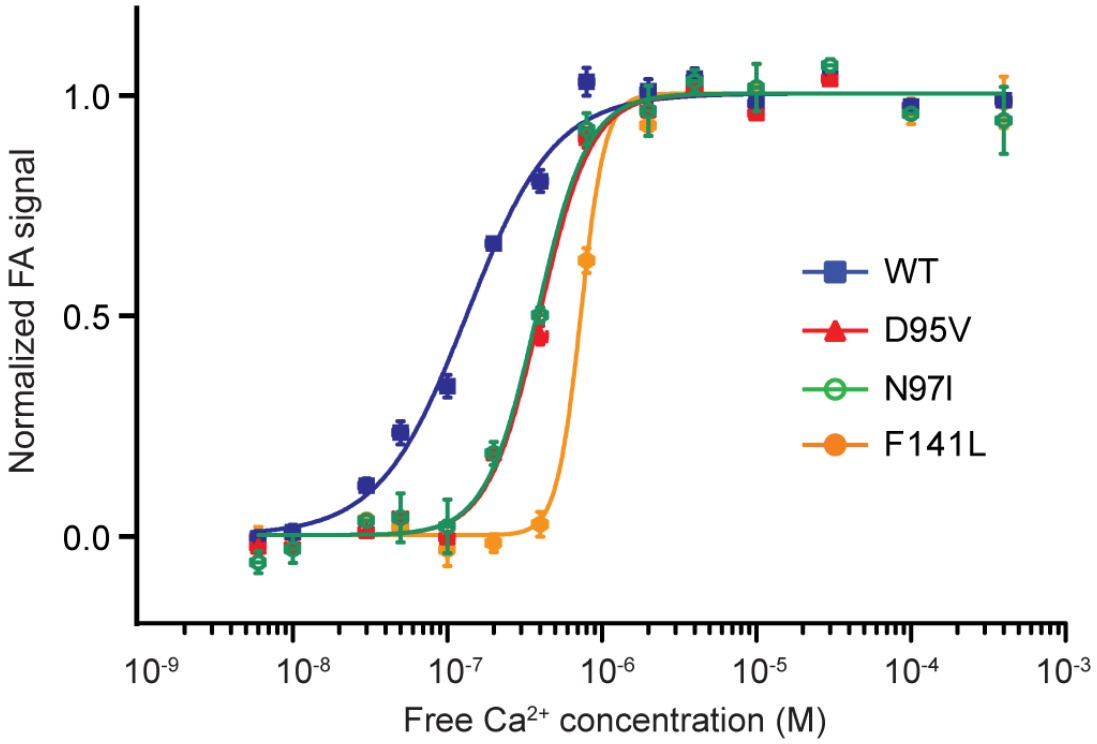

Supplementary Figure 3. Ca^{2+} binding to CaM:IQ complexes. Normalized TAMRA fluorescence anisotropy of CaM:IQ complexes as a function of the free Ca^{2+} concentration. Ca^{2+} binding curves were fit to a Hill model. Error bars represent the standard deviation of three replicates. Hill-fit gives the following Ca^{2+}-Kd values (with standard deviations): WT = 134±5 nM, D95V = 397±12 nM, N97I = 381±15 nM, F141L = 732±16 nM. The N97S mutant did not display a significant change in FA values and was therefore not plotted. The error on free Ca^{2+} was estimated at 10% (see SI Appendix, Supplementary Methods) and indicated as a horizontal error bar, just larger than the symbols.

Figure S4

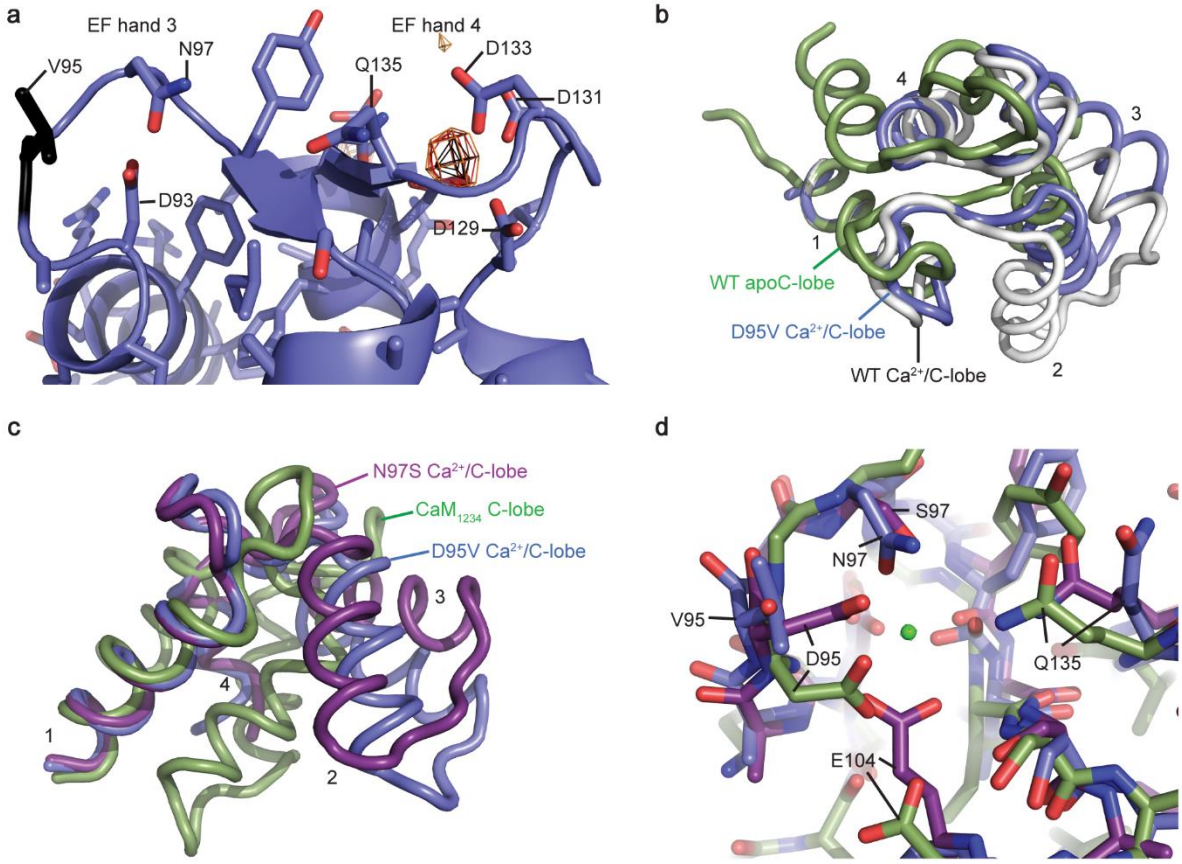

Supplementary Figure 4 (a) Overview of the anomalous difference Fourier map for calcium ions in the C-lobe of the D95V Ca^{2+}/CaM:IQ domain structure. D95V Ca^{2+}/CaM is shown in cartoon and stick representation, with the V95 residue colored in black. The anomalous difference electron density is contoured at 3σ (orange mesh), 4σ (red mesh), and 5σ (black mesh). **(b)** Superposition of the C-lobes of WT apoCaM (PDB 4DCK, green), WT Ca^{2+}/CaM:IQ (PDB 2BE6) and D95V Ca^{2+}/CaM:IQ (blue). The superposition is based on the first helix of the lobes, highlighting the completely different conformation of D95V compared to either WT C-lobe. **(c)** Comparison of the Clobes of D95V Ca^{2+}/CaM:IQ (blue), N97S Ca^{2+}/CaM (magenta), and CaM_{1234} (green; PDB 5TP5). The superposition is based on the first helix of the lobes. **(d)** Comparison of the EF hand 3 region of D95V Ca^{2+}/CaM:IQ (blue), N97S Ca^{2+}/CaM (magenta), and CaM_{1234} (green; PDB 5TP5). The superposition is based on the loop in EF hand 3 (residues 93-102).

Figure S5

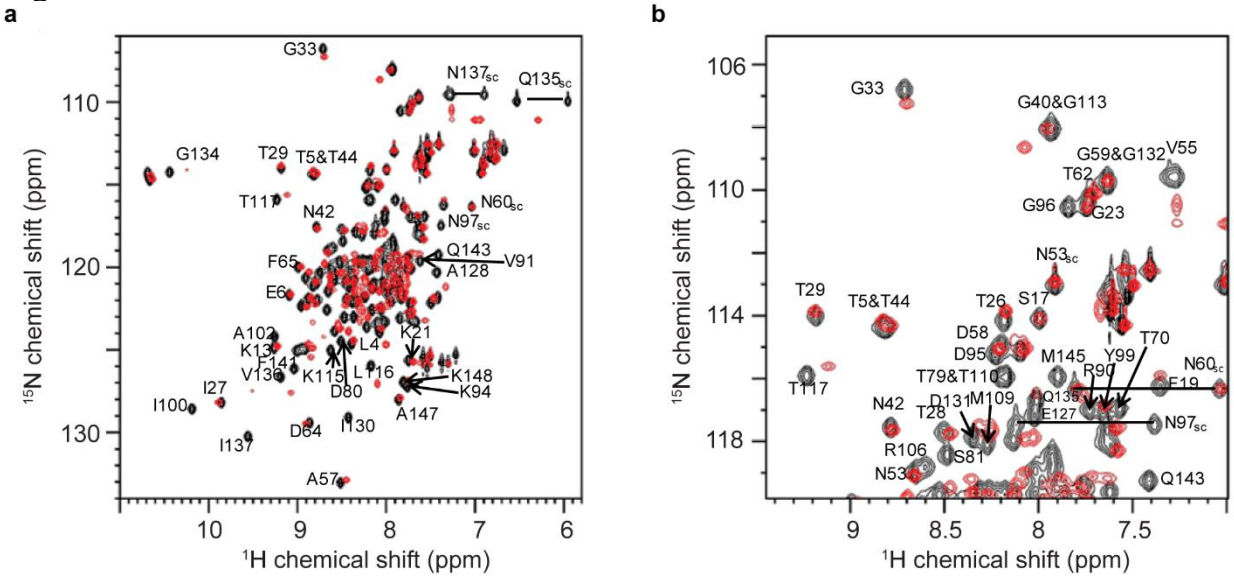

Supplementary Figure 5: Comparison of [^{1}H,^{15}N]-HSQC NMR spectra of wild-type Ca^{2+}/CaM (black) and D95V Ca^{2+}/CaM (red). **(a)** The whole spectrum and **(b)** a zoom of the region containing the resonance of residue 95. Amino acid labels denote the assignment of the wild-type (black) spectrum. Subscript "sc" in the label denotes side-chain resonances. The two signals from amide side-chains are connected by a horizontal dashed line. The chemical shifts of residues of the linker region and the C-lobe of calmodulin are changed completely by the mutation, while the chemical shifts of N-lobe residues are only slightly affected.

Figure S6

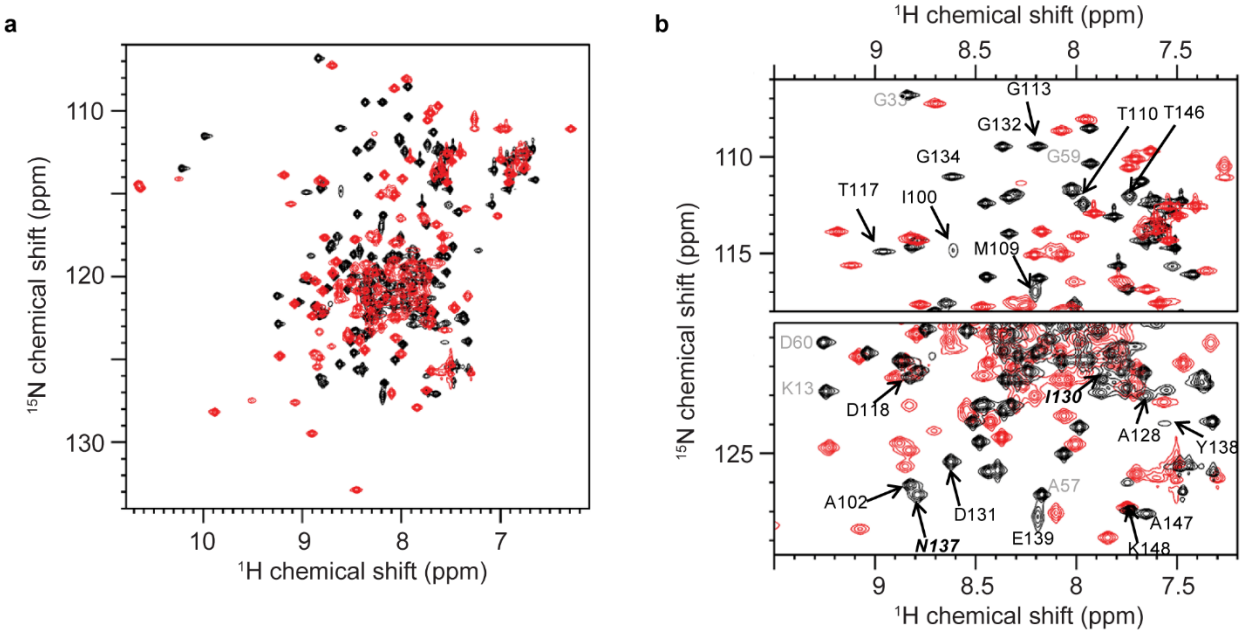

Supplementary Figure 6: Comparison of [^{1}H,^{15}N]-HSQC NMR spectra of the *apo*-wild-type (black) and Ca^{2+}-loaded D95V (red) calmodulin. **(a)** The whole spectrum and **(b)** two zooms. Amino acid labels denote the assignment of the wild-type (black) spectrum. N-lobe resonances are labelled in grey. Resonances of residues 128-140 constituting the intact fourth calcium binding site are highlighted in bold italics. The chemical shifts of C-lobe residues of the C-domain of calmodulin are changed completely showing that D95V, despite its lower Ca^{2+}-affinity, does not retain the structure of the *apo*-form under high Ca^{2+} concentrations.

Figure S7

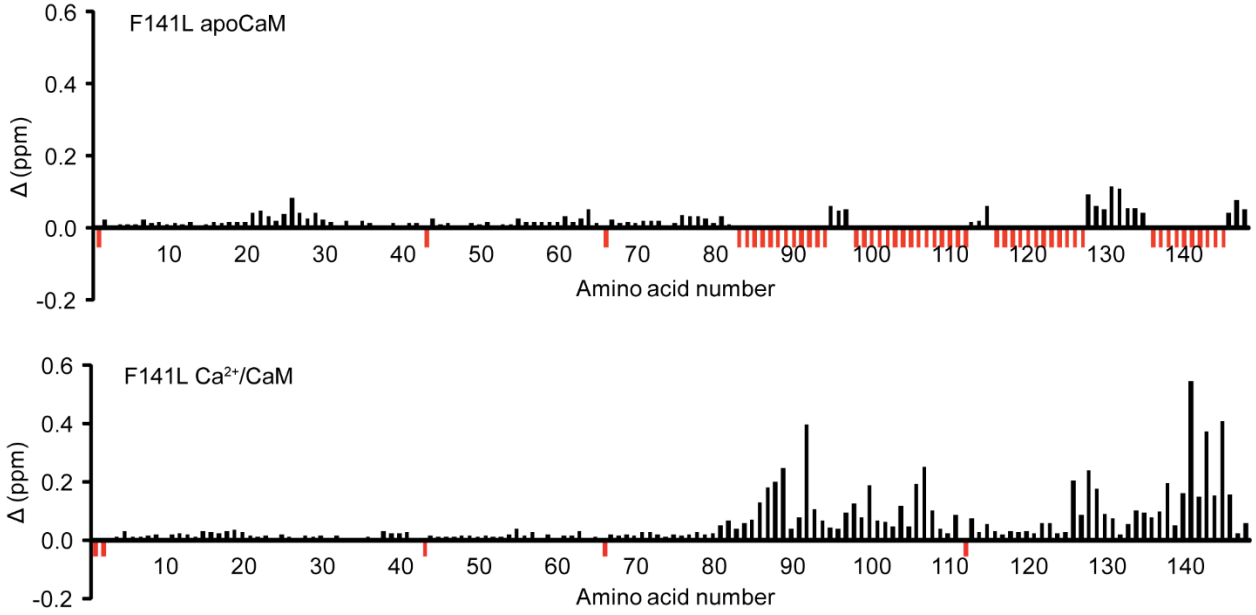

Supplementary Figure 7. Chemical shift differences between wild-type and F141L CaM in the *apo* **(a)** and Ca^{2+}-bound **(b)** forms. Chemical shift differences are calculated as $\Delta = \sqrt{\Delta\delta_H^2 + \left(\frac{\Delta\delta_N}{6.5}\right)^2}$, where $\Delta\delta_H$ and $\Delta\delta_N$ are the chemical shift changes of the hydrogen and nitrogen resonances, respectively, measured in ppm, and 6.5 is a generally accepted weighting factor(13). Red bars with values of -0.05 indicate that a peak for the given residue was not assigned in at least one of the two calmodulin variants or that the given amino acid is a proline without H^N.

Figure S8

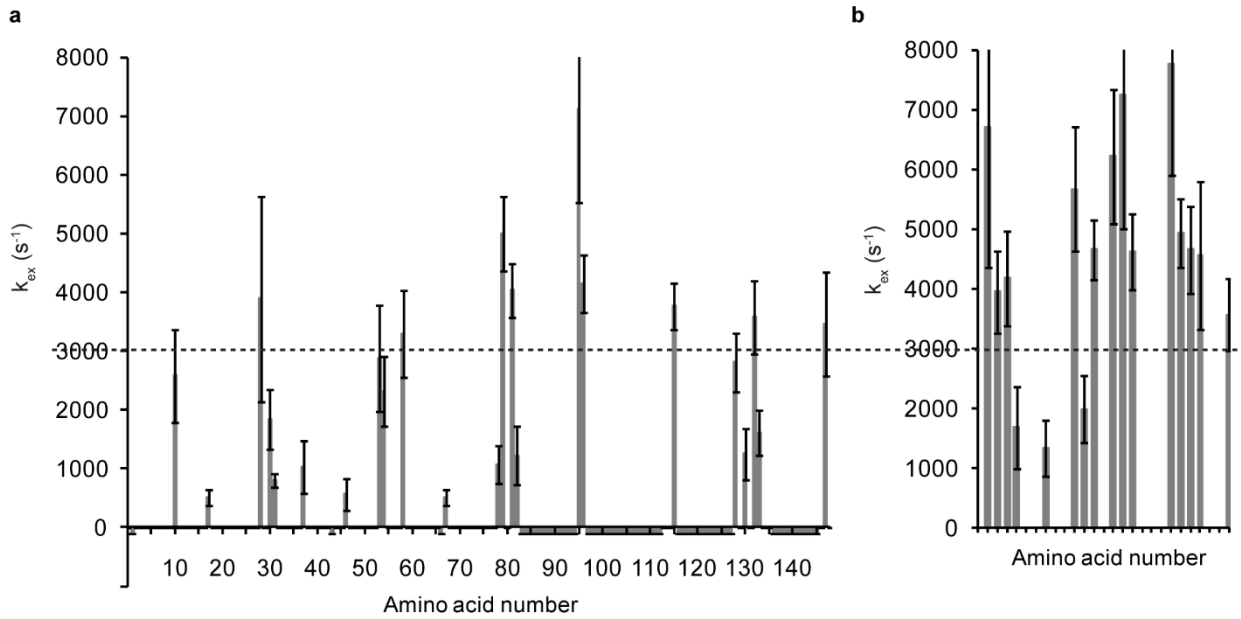

Supplementary Figure 8. rates of intrinsic exchange obtained from T_2 relaxation dispersion experiments with τ_{CPMG} = 50 ms. **(a)** k_{ex} vs amino acid sequence for those resonances that could be assigned. Unassigned amino acids are given the value k_{ex} = -100 s^{-1} in order to clearly distinguish them from amino acids without detectable relaxation dispersion. In the N-lobe, only Ala 1, Pro 43 and Pro 66 are left unassigned, while most of the C-lobe amino acids are unassigned. **(b)** k_{ex} values that could be determined for unassigned resonances belonging to the C-lobe. Error bars are given as 95% confidence interval as supplied by Mathematica. Values above ≈ 3000 s^{-1} cannot be determined reliably with this method(14)– this limit is indicated by the horizontal, dashed, black line. It can, however, be assumed that $k_{ex} \geq 3000$ s^{-1} for all those amino acids.

Figure S9

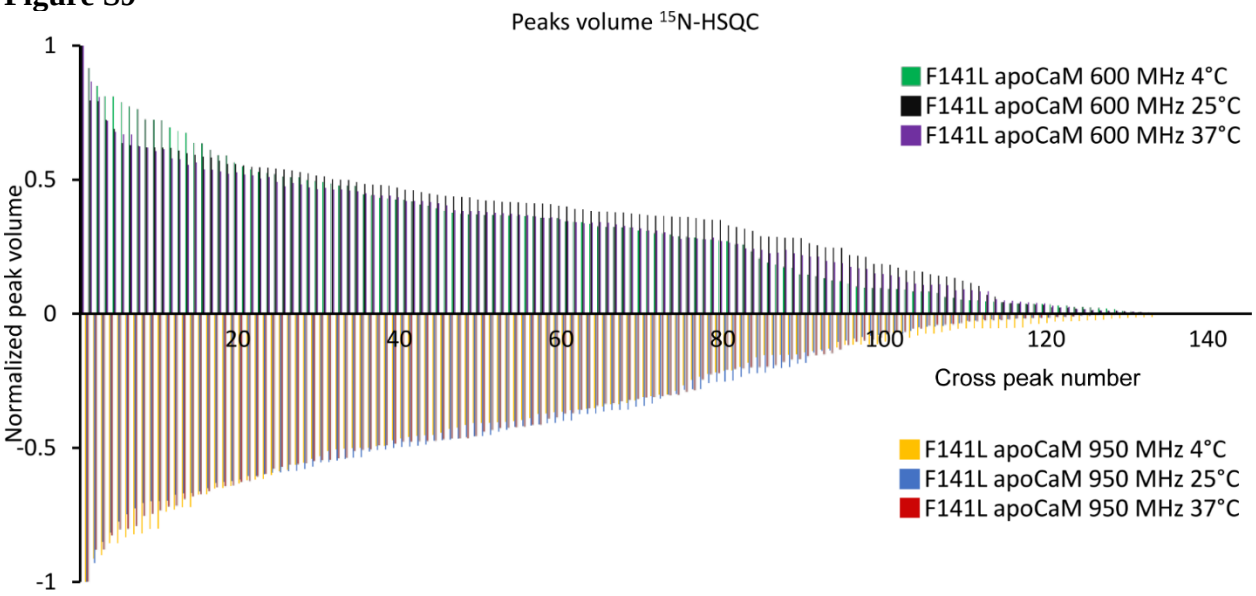

Supplementary Figure 9. Comparison of F141L apoCaM [^{1}H-^{15}N]-HSQC spectra recorded at different field strengths and temperatures. In each spectrum, each visible backbone amide peak was picked, integrated and then normalized to the strongest peak. Along the positive y-axis are spectra recorded at 600 MHz at the temperature 4 °C (green bars), 25 °C (black bars), and 37 °C (purple bars). Spectra recorded at 950 MHz are shown on the negative y-axis merely for readability with the temperatures 4 °C (yellow bars), 25 °C (blue bars), and 37 °C (red bars). The values are sorted by descending volume, i.e. their x-coordinate does not correspond to any specific residue number. It is seen that the peak volume profile for the HSQC spectra is very similar for all six spectra. The first ~77 peaks corresponding to roughly half of the amino acids in CaM display an expected intensity distribution. After that, intensities quickly drop. Hardly more than ~120 peaks are discernible from noise. Under all conditions tested here, the number of peaks is significantly smaller than the expected 145, and much smaller than what can be observed from the wild-type (see Figure 6c).

Figure S10

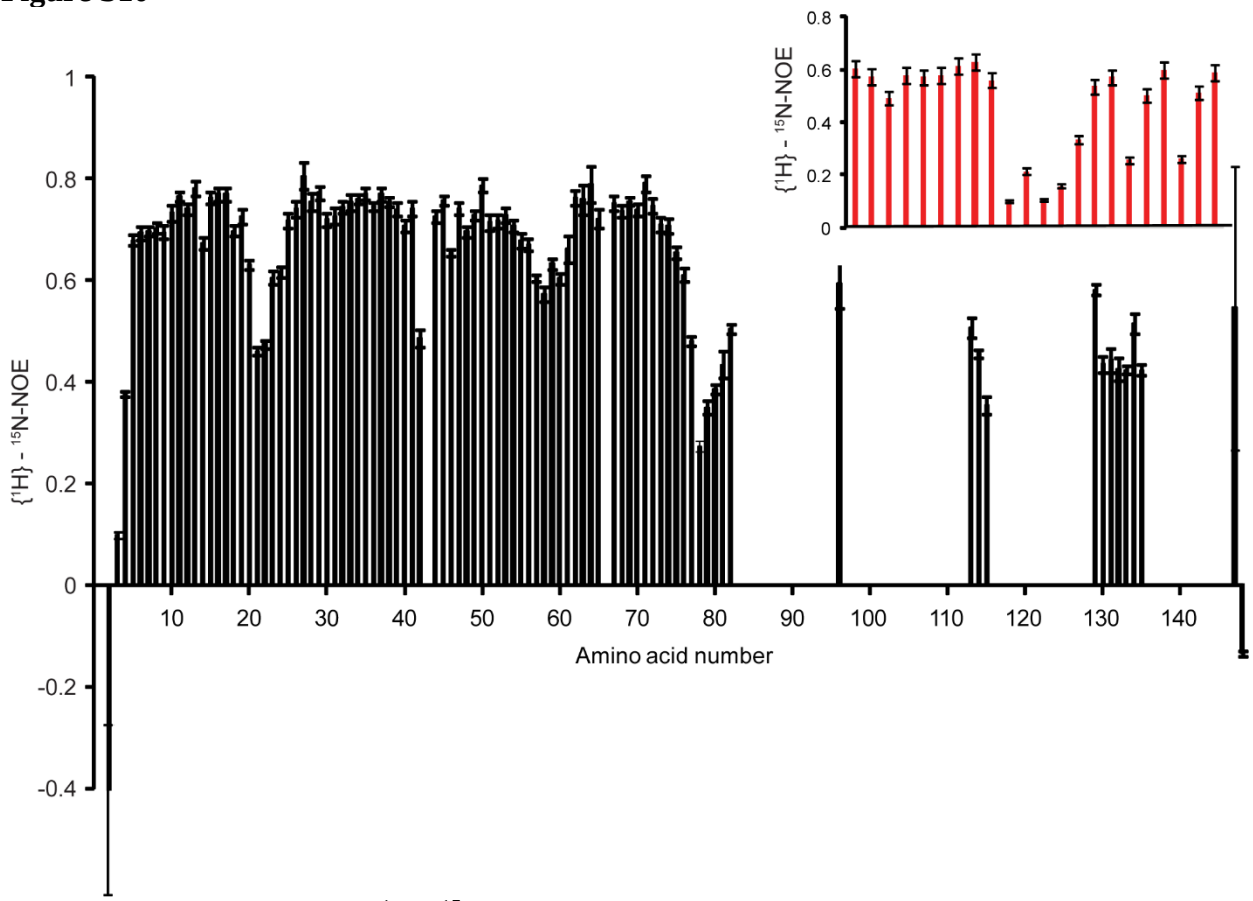

Supplementary Figure 10. $\{^{1}H\}$-^{15}N heteronuclear NOE values of F141L apoCaM. Lower values indicate higher mobility. Missing values indicate either the absence of H^N (proline residues 43 and 66) or a missing resonance assignment. The insert with red bars in panel A shows measurable NOEs from C-lobe residues of F141L apoCaM, that could not be assigned. They all exhibit higher intramolecular mobility than can be expected in well-ordered regions of the protein molecule.

Figure S11

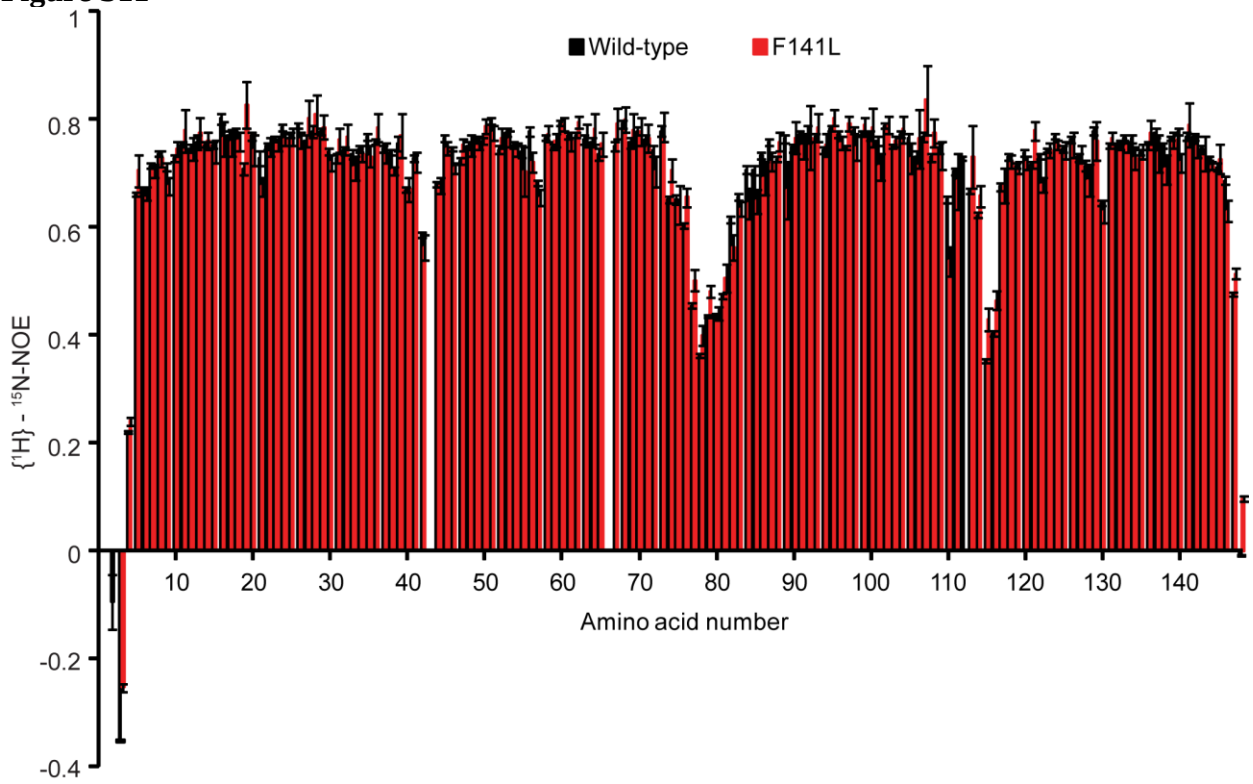

Supplementary Figure 11. $\{^{1}H\}$-^{15}N-NOE values (shown as intensity ratio between a spectrum recorded with ^{1}H-saturation and a spectrum recorded without ^{1}H saturation) for fully Ca^{2+} loaded wild-type (black) and F141L (red) CaM. The estimated error of fitting is shown as error bars. Lower values indicate higher mobility. Missing values indicate either the absence of H^{N} (proline residues 43 and 66) or a missing resonance assignment (amino acid 1 in both proteins and amino acids 2 and 112 in F141L).

Figure S12

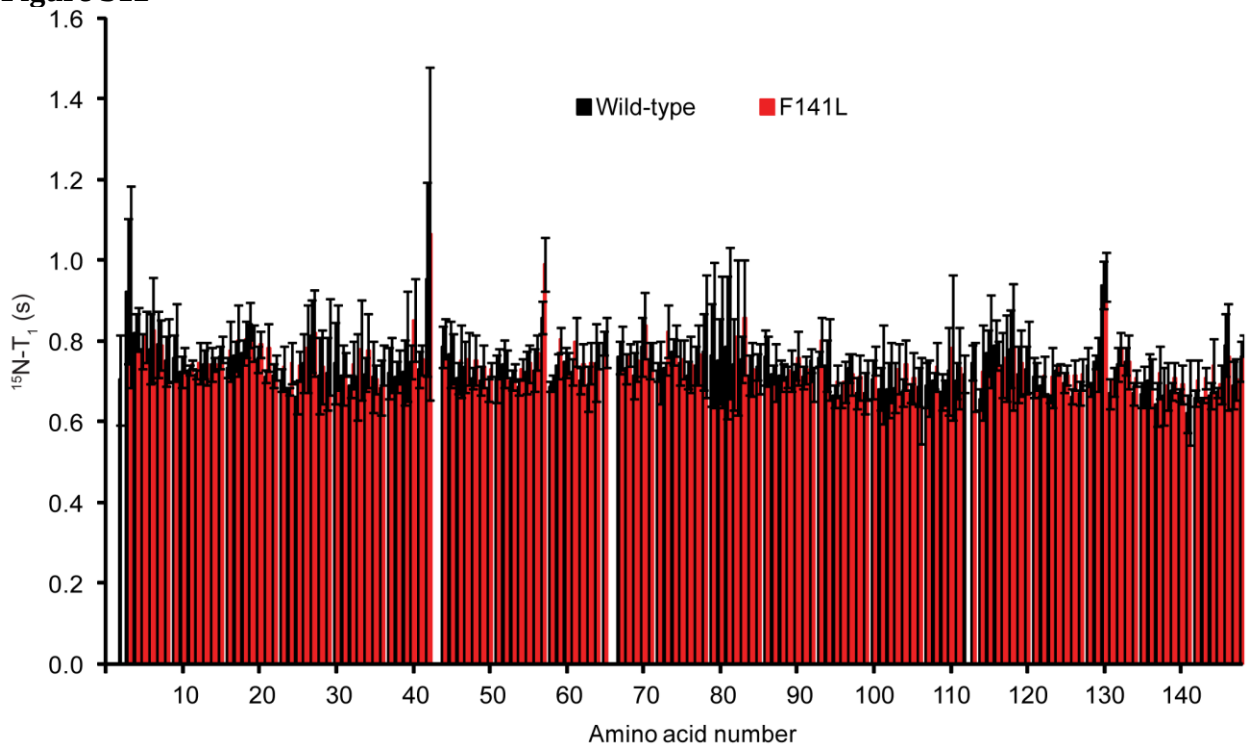

Supplementary Figure 12: ^{15}N-T_1 values for fully Ca^{2+} loaded wild-type (black) and F141L (red) CaM. The estimated error of fitting is shown as error bars. Missing values indicate either the absence of H^N (proline residues 43 and 66) or a missing resonance assignment (amino acid 1 in both proteins and amino acids 2 and 112 in F141L).

Figure S13

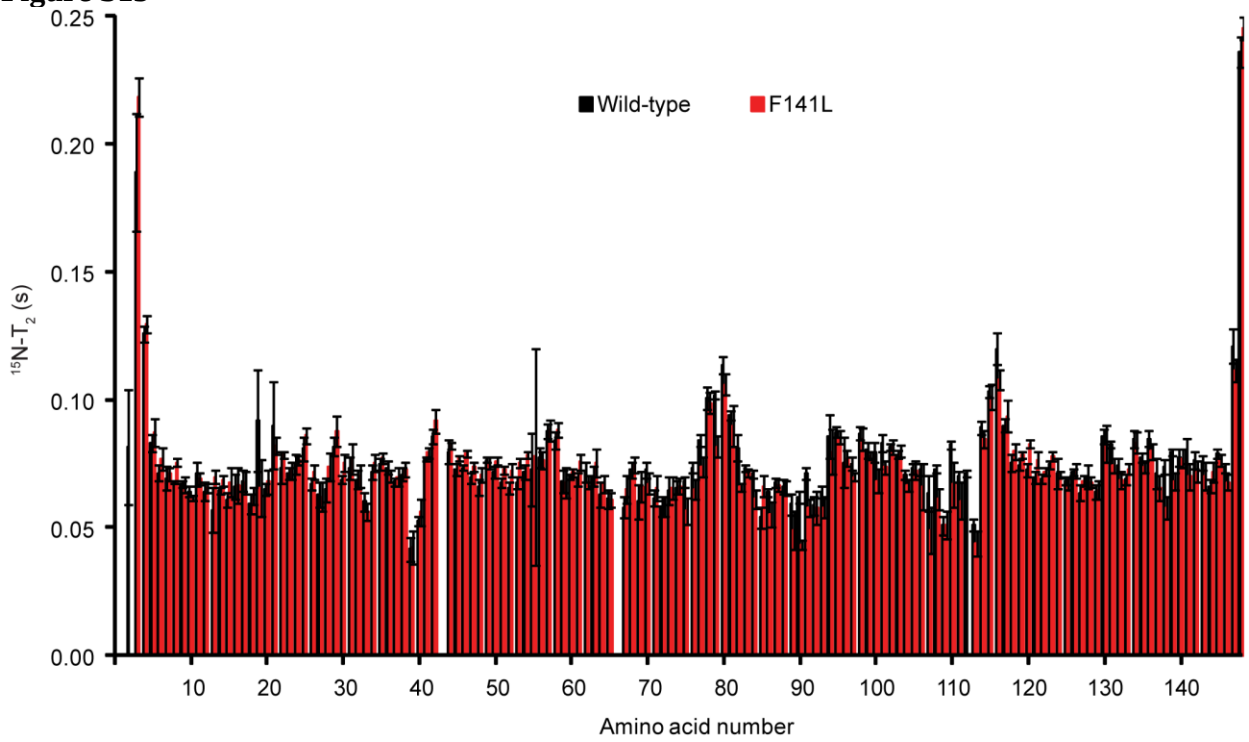

Supplementary Figure 13: ^{15}N-T$_2$ values for fully Ca^{2+} loaded wild-type (black) and F141L (red) CaM. The estimated error of fitting is shown as error bars. Missing values indicate either the absence of H^N (proline residues 43 and 66) or a missing resonance assignment (amino acid 1 in both proteins and amino acids 2 and 112 in F141L).

SUPPLEMENTARY TABLES

Table S1. Binding affinities of the Ca^{2+}-free and Ca^{2+}-saturated CaM:IQ and C-lobe:IQ complexes

	Full length CaM		C-lobe CaM	
	Low Ca^{2+} (μM)	High Ca^{2+} (nM)	Low Ca^{2+} (μM)	High Ca^{2+} (nM)
WT	3.38±0.37	1.76±0.51	7.16±1.15	9.30±0.97
D95V	3.97±0.26	4.02±0.28	6.71±0.69	66.9±10.2
N97I	3.60±0.30	4.99±2.49	10.7±0.6	76.8±33.3
N97S	3.06±0.21	1.73±0.82	13.0±1.58	8.39±0.84
F141L	0.41±0.01	1.63±0.92	0.97±0.05	13.9±1.04

Apparent dissociation constants ($K_{D,app}$) of full length CaM:IQ and C-lobe:IQ complexes at low Ca^{2+} (3 nM) or high Ca^{2+} (400 μM). Each value corresponds to the mean of at least three replicates (± s.d.). Note that units are given in μM for low Ca^{2+} conditions and in nM for high Ca^{2+} conditions.

Table S2 Thermodynamic parameters for $Ca_V1.2$ IQ domain-Ca^{2+}/C-lobe interactions

	Ca^{2+}/C-lobe:IQ	D95V Ca^{2+}/C-lobe:IQ	N97I Ca^{2+}/C-lobe:IQ	N97S Ca^{2+}/C-lobe:IQ	F141L Ca^{2+}/C-lobe:IQ
N	1.00 ± 0.05	0.97 ± 0.15	1.08 ± 0.14	1.00 ± 0.08	0.96 ± 0.10
K_D (nM)	6.72 ± 5.47	2.37 ± 1.24	23.44 ± 7.72	9.46 ± 1.74	11.31 ± 0.79
ΔH (kcal mol^{-1})	-9.84 ± 0.46	-15.34 ± 0.39	-7.42 ± 0.18	-10.26 ± 0.15	-8.02 ± 0.76
ΔS (cal mol^{-1} K^{-1})	4.81 ± 2.84	-11.80 ± 1.97	10.10 ± 0.53	2.31 ± 0.59	9.43 ± 2.59
ΔG (kcal mol^{-1})	-11.27 ± 0.45	-11.82 ± 0.30	-10.43 ± 0.21	-10.95 ± 0.11	-10.83 ± 0.04

Thermodynamic parameters of wild-type Ca^{2+}/C-lobe, D95V Ca^{2+}/C-lobe, N97I Ca^{2+}/C-lobe, N97S Ca^{2+}/C-lobe, and F141L Ca^{2+}/C-lobe binding to the $Ca_V1.2$ IQ domain at pH 7.4 in the presence of 10 mM $CaCl_2$. Note the higher amount of Ca^{2+} compared to the "high Ca^{2+}" in Table S1 (400μM). Each value corresponds to the mean of three separate experiments (± s.d.).

Table S3 Data collection and refinement statistics

	D95V Ca^{2+}/CaM:IQ domain	N97I Ca^{2+}/CaM:IQ domain	N97S Ca^{2+}/CaM	F141L Ca^{2+}/CaM:IQ domain
Data collection				
Space group	*P2₁2₁2₁*	*P2₁2₁2₁*	*P2₁*	*P2₁2₁2₁*
Cell dimensions				
a, *b*, *c* (Å)	65.2, 69.7, 86.2	65.3, 69.0, 85.8	59.1, 94.3, 60.9	34.4, 121.3, 125.9
α, β, γ (°)	90.0, 90.0, 90.0	90.0, 90.0, 90.0	90.0, 94.4, 90.0	90.0, 90.0, 90.0
Resolution (Å)	50.0-2.0 (2.12-2.00)	50.0-1.65 (1.75-1.65)	50.0-2.5 (2.65-2.50)	50.0-2.4 (2.55-2.40)
R_{merge} (%)	11.5 (55.4)	4.9 (51.5)	4.1 (30.6)	4.8 (43.7)
R_{meas} (%)	13.4 (64.5)	5.7 (60.1)	5.7 (42.4)	5.7 (52.3)
$I/\sigma(I)$	9.84 (2.60)	14.82 (2.17)	14.23 (2.43)	13.31 (2.43)
$CC_{1/2}$	99.5 (79.0)	99.9 (80.4)	99.9 (84.5)	99.8 (86.9)
Completeness (%)	99.9 (99.7)	99.9 (99.7)	95.4 (93.6)	99.1 (98.8)
Redundancy	3.88 (3.83)	3.92 (3.74)	1.81 (1.77)	3.09 (3.18)
Refinement				
Resolution (Å)	43.0-2.0	41.51-1.65	47.2-2.5	43.7-2.4
No. reflections	51054	90084	43334	39391
R_{work} / R_{free}	17.63/22.61	18.04/20.84	21.81/27.90	20.30/24.30
No. atoms				
Protein	2659	2665	4249	2463
Ligand	6	6	16	8
Water	219	230	34	19
B factors				
Protein	26.8	32.4	56.9	79.0
Ligand	22.7	26.2	54.1	70.8
Water	29.3	36.2	46.9	59.8
R.m.s. deviations				
Bond lengths (Å)	0.006	0.006	0.007	0.007
Bond angles (°)	0.746	0.733	0.840	0.808

One crystal was used for structure solution. Highest resolution shell is shown in parentheses.

Table S4 Parameters of NMR structure determination of F141L apoCaM and Ca^{2+}/CaM

	F141L apoCaM	F141L Ca^{2+}/CaM
Number of distance restraints	937	1229
intraresidual (|i-j| = 0)	349	782
sequential (|i-j| = 1)	275	209
medium-range (2≤ |i-j| ≤ 4)	190	91
long range (|i-j| ≥ 5)	123	147
number of restraints to Calcium ions	N/A	24
Number of dihedral angle constraints derived by TALOS-N		
φ	68	126
ψ	68	126
Residual CYANA target function (before refinement)	0.79±0.11 $Å^2$	2.98±0.33 $Å^2$
Backbone RMSD from average		
N-domain: C', C^{α},N of residues 8-35 and 45-72	0.84±0.18 Å	0.65±0.24 Å
C- domain (C', C^{α},N of residues 89-110 and 118-145)	N/A	0.47±0.07 Å
Heavy atoms RMSD from average		
N-domain: residues 8-35 and 45-72	1.28±0.17 Å	0.95±0.20 Å
C- domain (C', C^{α},N of residues 89-110 and 118-145)	N/A	0.99±0.13 Å
Ramachandran plot as given by PROCHECK-NMR		
residues in most favored regions	93.7%	92.5%
residues in additionally allowed regions	6.1%	7.5%
residues in generously allowed regions	0.2%	0.0%
residues in forbidden regions	0.0%	0.0%

TABLE S5: Summary of findings per mutant

Mutation	**N97S**	**D95V**	**N97I**	**F141L**
Associated disease	CPVT, LQT	LQT	LQT	LQT
Affinity for IQ domain in low Ca^{2+} (relative to WT)	Similar	Similar	Similar	10-fold higher. This implies a higher degree of preassociation with the IQ domain.
Affinity for IQ domain in high (400 µM) Ca^{2+}(relative to WT)[$]	Similar	~2-fold weaker	~2-fold weaker	Similar
Affinity of Ca^{2+} for the mutant CaM/IQ complex (relative to WT)	Could not be measured	~3-fold weaker	~3-fold weaker	~5.5-fold weaker
Effects on structure	Small distortion in EF 3 that likely lowers Ca^{2+} affinity	Abolishes Ca^{2+} binding to EF3 Major conformational changes in the Ca^{2+}/C-lobe. Altered interactions with the IQ domain that fully sequester Ile1624.	Abolishes Ca^{2+} binding to EF3 Major conformational changes in the Ca^{2+} C-lobe. Altered interactions with the IQ domain that fully sequester Ile1624.	Minimal changes in the Ca^{2+}/C-lobe. Similar interactions with IQ domain, but with decreased hydrophobic packing. Large conformational changes in the Ca^{2+} free form as indicated by NMR and Native PAGE.

[$] based on TAMRA fluorescence experiments

SUPPLEMENTARY MOVIES

Movie S1
Morph video showing a close-up in the EF3 region. The animation morphs between the wild-type and D95V Ca^{2+}/CaM:IQ complexes. The calcium ion is shown as a green sphere. Oxygen atoms are shown in red. The mutated residue is shown in black. Glu104, which swings away from the site, is highlighted in orange.

Movie S2
Morph video showing the conformational changes in the Ca^{2+}/C-lobe due to the D95V mutation. The animation morphs between the wild-type and D95V Ca^{2+}/CaM:IQ complexes. The calcium ion is shown as a green sphere. Oxygen atoms are shown in red. The mutated residue is shown in black. Glu104, which swings away from the site, is highlighted in orange. Two different views are shown, with the second view showing the hydrophobic face that normally interacts with the IQ domain. The IQ domain and N-lobe have been omitted for clarity.

Movie S3
Morph video showing a close-up in the EF3 region. The animation morphs between wild-type and N97S Ca^{2+}/CaM. The calcium ion is shown as a green sphere. Oxygen atoms are shown in red. The mutated residue is shown in black. The Ser97 hydroxyl group can compensate for the loss of a Ca^{2+}-coordinating residue, and Ca^{2+} binding is thus retained. However, the side chain moves in closer, likely resulting in strain that underlies the weakened affinity.

SUPPLEMENTARY REFERENCES

1. Farrow NA, *et al.* (1994) Backbone dynamics of a free and phosphopeptide-complexed Src homology 2 domain studied by 15N NMR relaxation. *Biochemistry* 33(19):5984-6003.
2. Tollinger M, Skrynnikov NR, Mulder FA, Forman-Kay JD, & Kay LE (2001) Slow dynamics in folded and unfolded states of an SH3 domain. *Journal of the American Chemical Society* 123(46):11341-11352.
3. Vranken WF, *et al.* (2005) The CCPN data model for NMR spectroscopy: development of a software pipeline. *Proteins* 59(4):687-696.
4. Shen Y & Bax A (2013) Protein backbone and sidechain torsion angles predicted from NMR chemical shifts using artificial neural networks. *J Biomol NMR* 56(3):227-241.
5. Guntert P & Buchner L (2015) Combined automated NOE assignment and structure calculation with CYANA. *J Biomol NMR* 62(4):453-471.
6. Guntert P (1997) Calculating protein structures from NMR data. *Methods Mol Biol* 60:157-194.
7. Guntert P, Mumenthaler C, & Wuthrich K (1997) Torsion angle dynamics for NMR structure calculation with the new program DYANA. *Journal of molecular biology* 273(1):283-298.
8. Herrmann T, Guntert P, & Wuthrich K (2002) Protein NMR structure determination with automated NOE-identification in the NOESY spectra using the new software ATNOS. *J Biomol NMR* 24(3):171-189.
9. Keller R (2004) *The computer aided resonance assignment tutorial*.
10. Krieger E & Vriend G (2014) YASARA View - molecular graphics for all devices - from smartphones to workstations. *Bioinformatics* 30(20):2981-2982.
11. Krieger E, Koraimann G, & Vriend G (2002) Increasing the precision of comparative models with YASARA NOVA--a self-parameterizing force field. *Proteins* 47(3):393-402.
12. Krieger E, *et al.* (2009) Improving physical realism, stereochemistry, and side-chain accuracy in homology modeling: Four approaches that performed well in CASP8. *Proteins* 77 Suppl 9:114-122.
13. Mulder FA, Schipper D, Bott R, & Boelens R (1999) Altered flexibility in the substrate-binding site of related native and engineered high-alkaline Bacillus subtilisins. *Journal of molecular biology* 292(1):111-123.
14. Kleckner IR & Foster MP (2011) An introduction to NMR-based approaches for measuring protein dynamics. *Biochim Biophys Acta* 1814(8):942-968.